Available online at www.sciencedirect.com
SCIENCE DIRECT®
International Journal of Thermal Sciences 44 (2005) 374–381
International Journal of Thermal Sciences
www.elsevier.com/locate/ijts

# A new type of the boundary condition allowing analytical solution of the thermal boundary layer equation

Igor V. Shevchuk [1]

*Institut für Luft- und Raumfahrttechnik, Technische Universität Dresden, 01062, Dresden, Germany*

Received 20 October 2004; accepted 20 October 2004

**Abstract**

Outlined in this paper is a new analytical form of a non-monotone distribution of the wall temperature allowing solving the thermal boundary layer equation analytically. The thermal boundary layer equation in its integral form was solved for the temperature distribution at the wall, with the Nusselt number being specified as a boundary condition in the form of an arbitrary power-law function. The new solution, as illustrated on the example of a free rotating disk, can provide the analytical formulas for the wall temperature distributions having points of a maximum or a minimum, while the traditionally used power-law distributions behave as the monotone functions. The new solution includes earlier known power-law solutions for the wall temperature and the Nusselt number as a particular case. Numerical data computed using the proposed solution are in a better agreement with known experimental data than the traditionally used power-law functions.


*Keywords:* Heat transfer; Rotating disk; Analytical solution; Boundary layer

## 1. Introduction

At present, the most part of the approximate analytical solutions of the equations of laminar and turbulent thermal boundary layers are known to be obtained using a power-law distribution for the wall temperature considered as a boundary condition of the problem. For a free rotating disk taken in the present research as an example (see Fig. 1), the power-law distribution of the wall temperature, as specified by Dorfman [1] can be written in the following form

$$T_w - T_\infty = c_0 r^{n_*} \tag{1}$$

$$\overline{\Delta T} = c_0^* x^{n_*} \tag{2}$$

where $n_*$, $c_0$, and $c_0^*$ are constants. If distribution (2) is valid at any $x$, then $c_0^* = 1$. In the case if Eq. (2) holds only within a certain range of variation of the argument $x$, the constant $c_0^*$ can be chosen in an empirical way and differs from unity.

The Nusselt number for boundary conditions (1), (2) is featured by relation

$$Nu = K_1 Re_\varphi^{n_R} x^{1+m} \tag{3}$$

Values of constants and exponents in Eq. (3) were obtained both experimentally and theoretically by Cardone et al. [2], Dorfman [1], Elkins and Eaton [3], Owen and Rogers [4,5] etc. Currently known integral methods (laminar and turbulent flow) and self-similar solution (laminar flow) state the following unique relation between the exponents in Eq. (3)

$$m = 2n_R - 1 \tag{4}$$

where $m = 0$ for laminar flow, and most often $m = 0.6$ for turbulent flow.

Constant $K_1$ depends on the type of the boundary conditions at the wall, flow regime and Prandtl number. The most widely known and frequently cited solution for the constant $K_1$ is that of Dorfman [1]. Corrected by Owen and Rogers [4] for turbulent flow it looks as

$$K_1 = 0.0197(n_* + 2.6)^{0.2} Pr^{0.6} \tag{5}$$

*E-mail address:* ivshevch@tfd.mw.tu-dresden.de (I.V. Shevchuk).
[1] Fax: 49 (351) 463 38087, tel.: 49 (351) 463 38099.

1290-0729/$ – see front matter 
doi:10.1016/j.ijthermalsci.2004.10.004

**Nomenclature**

| | |
|---|---|
| $b$ | outer radius of the disk ..... m |
| $C_f/2$ | total skin friction coefficient, $=\tau_w/(\rho V_*^2)$ |
| $c_p$ | specific heat at constant pressure .. $\mathrm{J\cdot kg^{-1}\cdot K^{-1}}$ |
| $k$ | thermal conductivity ..... $\mathrm{W\cdot m^{-1}\cdot K^{-1}}$ |
| $K_V$ | shape-factor of the velocity profile, $=\int_0^\infty v_r v_\varphi \,\mathrm{d}z/[\omega r \int_0^\infty v_r \,\mathrm{d}z]$ |
| $m$ | parameter, $=(1-n)/(3n+1)$ |
| $m_x$ | arbitrary exponent in Eq. (9) |
| $m_x^*$ | parameter, $=m_x - m$ |
| $Nu$ | local Nusselt number, $=q_w r/[k(T_w - T_\infty)]$ |
| $n$ | exponent in the approximation of the velocity and temperature profiles in turbulent flow, Eqs. (18), (19) |
| $n_R$ | exponent of the Reynolds number in Eqs. (3), (9) |
| $n_*$ | exponent in the radial distribution of the wall temperature, Eq. (1), (2) |
| $Pr$ | Prandtl number, $=\mu c_p/k$ |
| $q_w$ | heat flux at the wall ..... $\mathrm{W\cdot m^{-2}}$ |
| $Re_\omega$ | local rotational Reynolds number, $=\rho\omega r^2/\mu$ |
| $Re_\varphi$ | rotational Reynolds number at the outer radius of disk, $=\rho\omega b^2/\mu$ |
| $Re_{V_*}$ | modified rotational Reynolds number, $=\rho V_* \delta/\mu$ |
| $r, \varphi, z$ | radial, tangential and axial cylindrical coordinates ..... m |
| $T$ | temperature ..... K |
| $\mathrm{tg}\,\varphi$ | tangent of the flow swirl angle, $=v_r/(\omega r - v_\varphi)$ |
| $v_r, v_\varphi, v_z$ | radial, tangential and axial velocity components in cylindrical coordinates .. $\mathrm{m\cdot s^{-1}}$ |
| $V_*$ | $=\omega r(1+\alpha^2)^{1/2}$ modified velocity ..... $\mathrm{m\cdot s^{-1}}$ |
| $x$ | dimensionless radial coordinate, $=r/b$ |

*Greek symbols*

| | |
|---|---|
| $\alpha$ | wall value of the tangent of the flow swirl angle $\mathrm{tg}\,\varphi$ |
| $\Delta$ | ratio of thickness of the thermal boundary layer to thickness of the boundary layer, $=\delta_T/\delta$ |
| $\delta, \delta_T$ | thickness of boundary layer and thermal boundary layer, respectively ..... m |
| $\bar{\delta}$ | dimensionless boundary layer thickness, $=\delta/b$ |
| $\Delta T$ | temperature difference between the wall and the outer flow, $=T_w - T_\infty$ ..... K |
| $\overline{\Delta T}$ | dimensionless temperature difference, $=\Delta T/\Delta T_{x=1}$ |
| $\Delta T_{x=1}$ | temperature difference at $x=1$ ..... K |
| $\mu$ | dynamic viscosity ..... Pa·s |
| $\xi$ | dimensionless coordinate, $=z/\delta$ |
| $\xi_T$ | dimensionless coordinate, $=z/\delta_T$ |
| $\rho$ | density ..... $\mathrm{kg\cdot m\,s^{-3}}$ |
| $\tau_w$ | total shear stress at the wall ..... Pa |
| $\chi$ | Reynolds analogy parameter |
| $\omega$ | angular speed of rotation ..... $\mathrm{s^{-1}}$ |

*Subscripts*

| | |
|---|---|
| crit | critical point |
| ext | point of extremum |
| $r, \varphi$ | radial and angular projections of a parameter |
| $w$ | wall |
| $\infty$ | outer edge of the boundary layer |

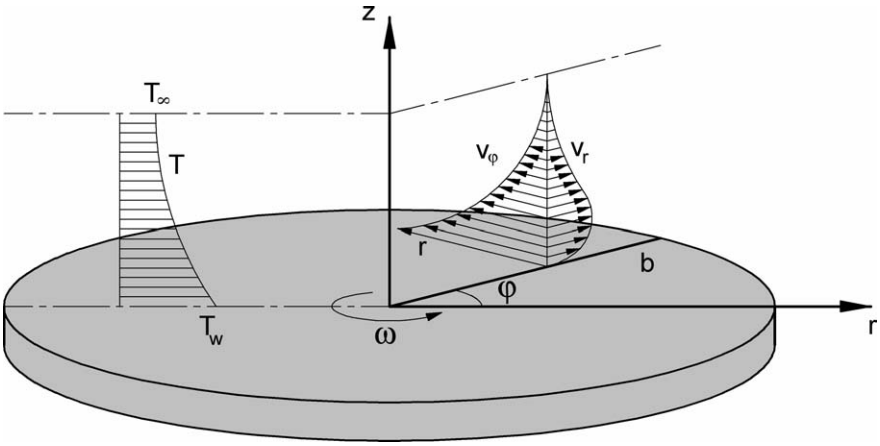


Fig. 1. Layout of the problem under investigation.

at $n_R = 0.8$, $m = 0.6$, $n = 1/7$.

Dorfman's solution agrees well with early experiments of Cobb and Saunders [6] and Nikitenko [7]. However, Eq. (5) noticeably (in certain cases up to 14%) overpredicts results of the more careful experimental investigations of Cardone et al. [2], Elkins and Eaton [3], McComas and Hartnett [8], Northrop [9], Northrop and Owen [10], Popiel and Boguslawski [11] fulfilled later for the values of $n_* = -1, \ldots, 0$ (i.e., at $\mathrm{d}\overline{\Delta T}/\mathrm{d}x \leqslant 0$). Shevchuk [12] has shown that Dorfman's (1963) solution for the laminar flow

Table 1
Values of constants in Eqs. (3), (7) for turbulent flow in accordance with Shevchuk [13]

| Coefficient | $n = 1/7$ | $n = 1/6.5$ | $n = 1/6$ |
|---|---|---|---|
| $K_3$ | 0.0268 | 0.0306 | 0.0353 |
| $K_V$ | 0.203 | 0.215 | 0.228 |
| $n_p = 0.4/(1 - K_V)$ | 0.502 | 0.509 | 0.518 |
| $n_R = (n + 1)/(3n + 1)$ | 0.8 | 0.789 | 0.778 |
| $m = (1 - n)/(3n + 1)$ | 0.6 | 0.579 | 0.556 |
| $m_x = 1 + m$ | 1.6 | 1.579 | 1.556 |

$$K_1 = K_2 = 0.308(n_* + 2)^{1/2} Pr^{1/2} \tag{6}$$

is in the even worse agreement with the self-similar solution at $n_* = -1.5, \ldots, 0$ for $Pr = 1, \ldots, 0.1$; inexactitudes of Eq. (6) reach 34, ..., 238% and increase with the decreasing Prandtl number.

The remedy was found by Shevchuk [12,13], whose solution (valid at $Pr \leqslant 1$) is

$$K_1 = K_3 Pr \left[ \frac{4 + m}{2 + m + n_*} K_V + (1 - K_V) Pr^{n_p} \right]^{-1} \tag{7}$$

$$K_1 = \frac{0.4435}{0.3486 + 2.002/(2 + n_*)} \tag{8}$$

Eq. (7) corresponds to turbulent flows, while Eq. (8) (presented here for the particular case of $Pr = 0.72$) is valid for laminar flows.

Numerical values of constants in Eq. (7) depending on the exponent $n$ in the power-law approximation of the temperature and velocity profiles (for details see Eqs. (18), (19)) are documented in Table 1. Eq. (7) (at the standard value of $n = 1/7$) and (8) agree very well with known experimental and theoretical data of Cardone et al. [2], Elkins and Eaton [3], McComas and Hartnett [8], Owen and Rogers [4], Popiel and Boguslawski [11], Shevchuk [12], for which the boundary conditions (1) and (2) are valid.

Sometimes the wall temperature distributions cannot be accurately described by analytical Eqs. (1) and (2), as for example, took place in experiments of Northrop [9], Northrop and Owen [10].

Distributions of the Nusselt number obtained by these authors also differ quite significantly from the values suggested by Eqs. (3), (5), (7) and experimental data of other authors. The main feature of the experimental values for *Nu* measured by Northrop [9], Northrop and Owen [10] is that they clearly exhibit a weaker dependence on the radial coordinate $x$, than that predicted by Eqs. (3) and (4) at $n = 1/7$.

Thus the aim of the present research was to find out, whether another class of the analytical solutions can be derived, which can be in a good agreement with experimental data of Northrop [9], Northrop and Owen [10] that do not comply reasonably good with boundary conditions (1), (2) and correspondent equations for the Nusselt number. The analysis below is performed in the general form suitable both for laminar and turbulent flow, however comparisons of the newly obtained solution is made only for the turbulent flow most often occurring in technical applications.

## 2. Statement of the problem

We are looking here for an opportunity to find out an approximate analytical solution of the rotating disk heat transfer problem for the case, where the exponent at variable $x$ in Eq. (3) takes an arbitrary value $m_x = \text{const}$, which is in general different from $1 + m$

$$Nu = K_1 Re_\varphi^{n_R} x^{m_x} \tag{9}$$

Most commonly the energy equation is solved for the temperature distributions in the fluid (and for the Nusselt numbers) at specified boundary conditions for the temperature at the wall. We will refer in this paper to this type of mathematical problems as direct ones. In order to derive an expression for the temperature distribution at the wall $\overline{\Delta T}$, which corresponds to Eq. (9), we will consider an inverse mathematical problem in the sense that the energy equation is to be solved for $\overline{\Delta T}$ at a given boundary condition for the Nusselt number in the form of Eq. (9).

Solution of the stated problem is performed using the integral method outlined in works of Shevchuk [12,13] and Shevchuk et al. [14]. An integral equation of the thermal boundary layer is

$$\frac{\mathrm{d}}{\mathrm{d}x}\left[ Re_\omega \bar{\delta} K_H K_m \overline{\Delta T} \right] = \frac{Nu}{Pr} \overline{\Delta T} \tag{10}$$

Parameters $K_H$ and $K_m$ are defined by Owen and Rogers [4] and Shevchuk [12,13] as

$$K_H = \int_0^\infty v_r (T - T_\infty)\, \mathrm{d}z \Big/ \left[ (T_w - T_\infty) \int_0^\infty v_r\, \mathrm{d}z \right] \tag{11}$$

$$K_m = \delta^{-1} \int_0^\delta \frac{v_r}{\omega r}\, \mathrm{d}z \tag{12}$$

As suggested by Owen and Rogers [4,5], integral parameters for the hydrodynamic part of the problem in the laminar flow can be found via integration of the self-similar solution for the free rotating disk

$$K_m = I_\infty \alpha \frac{1}{\delta (\omega/\nu)^{1/2}} = I_\infty \alpha \frac{1}{\gamma}, \quad \alpha = 0.8284 \tag{13}$$

$$I_\infty = 0.5338, \qquad \bar{\delta} = C_\delta^*, \quad C_\delta^* = \gamma\, Re_\varphi^{-1/2} \tag{14}$$

$$K_m \bar{\delta} = I_\infty \alpha\, Re_\varphi^{-1/2} \tag{15}$$

$$\frac{C_f}{2} = A_c Re_\omega^{-1/2} = A_c Re_\varphi^{-1/2} x^{-1}$$

$$A_c = 0.6159\left(1 + \alpha^2\right)^{-1/2} \tag{16}$$

$$Nu = \frac{C_f}{2} Re_\omega \left(1 + \alpha^2\right)^{1/2} Pr\, \chi \tag{17}$$

Choice of the values $C_\delta^*$ or $\gamma$ depends on the desired accuracy of their determination (via integration) from the self-similar profiles of $v_r$ and $v_\varphi$. Since parameters $\bar{\delta}$ and

$K_m$ are used in Eq. (9) as a product, chosen values of $C_\delta^*$ or $\gamma$ for laminar flow do not affect the subsequent transformations (see Eqs. (13)–(15)).

For turbulent flow, Shevchuk [13] used a power-law model for the velocity and temperature profiles in the following form

$$(v_\varphi - \omega r)/(-\omega r) = \xi^n$$
$$v_r/(\omega r) = \xi^n \operatorname{tg}\varphi = \alpha(1-\xi)^2\xi^n \tag{18}$$
$$(T - T_w)/(T_\infty - T_w) = \xi^n \tag{19}$$

The power-law model used by Shevchuk [12,13] for the Nusselt numbers is again Eq. (17), while the components of the shear stresses and the Reynolds analogy parameter are

$$\tau_{wr} = -\alpha\tau_{w\varphi}, \qquad \tau_{w\varphi} = -\tau_w\left(1+\alpha^2\right)^{1/2} \tag{20}$$
$$C_f = C_n^{-2/(n+1)} Re_{V_*}^{-2n/(n+1)} \tag{21}$$
$$\chi = \Delta^{-n} Pr^{-n_p} \tag{22}$$

where $C_n = 2.28 + 0.924/n$, $n_p = 0.4/(1-K_V)$. In Eq. (22) both $\chi$ and $\Delta$ are unknowns to be found from the solution of the thermal boundary layer equation.

The solution of Shevchuk [12,13] for the hydrodynamic parameters in the turbulent flow is

$$\bar\delta = C_\delta^* x^m, \qquad C_\delta^* = \gamma Re_\varphi^{-2n/(3n+1)} \tag{23}$$
$$\frac{C_f}{2} = A_c Re_\omega^{-2n/(3n+1)} = A_c Re_\varphi^{-2n/(3n+1)} x^{-4n/(3n+1)} \tag{24}$$
$$K_V = 1 - D_2/A_1, \qquad K_m = \alpha A_1$$
$$A_c = K_3\left(1+\alpha^2\right)^{-1/2} \tag{25}$$

We refer the reader who is interested in formulas for the rest of constants in Eqs. (23)–(25) to the work of Shevchuk [13] and references. Given $n = 1$ in Eqs. (23)–(25), one can obtain $m = 0$, with the exponent of the Reynolds number $Re_\varphi$ being equal to $-1/2$. Thus, Eqs. (23)–(25) formally generalize Eqs. (13)–(16) obtained for the analogous parameters of the laminar flow. However, it should be remembered that all constants for laminar flow are determined namely by Eqs. (13)–(16).

## 3. Solution of the inverse problem

Taking derivative of the left-hand part of Eq. (10) and dividing both sides of this equation by $Re_\omega\bar\delta K_H K_m\overline{\Delta T}$, one can deduce

$$\frac{\mathrm{d}}{\mathrm{d}x}\left[\ln\left(Re_\omega\bar\delta K_H K_m\overline{\Delta T}\right)\right] = \frac{Nu}{Pr}\frac{1}{Re_\omega\bar\delta K_H K_m} \tag{26}$$

It is necessary to integrate Eq. (26) from $x$ to 1 (provided that $x \neq 0$ to avoid uncertainty in both sides of this equation). Taking into account Eq. (9) for $Nu$ and (23) for $\bar\delta$, along with relation $Re_\omega = Re_\varphi x^2$, one can obtain

$$\left[\ln\left(Re_\omega\bar\delta K_H K_m\overline{\Delta T}\right)\right]_x^1 = \frac{K_1}{Pr\,K_m\gamma}\int_x^1 \frac{x^{m_x^*}\,\mathrm{d}x}{x^2 K_H} \tag{27}$$

Parameter $K_H$ is specified by the model of Shevchuk [12,13]

$$K_H = \frac{1}{b_2} - \chi\,Pr^{n_p}(1-K_V)\frac{b_1}{b_2} \tag{28}$$

For turbulent flow $b_1 = b_2 = 1$. For laminar flow, values of $b_1$, $b_2$ and $n_p$ depending only on the Prandtl number may be calculated using equations given in the work of Shevchuk [12] ($b_1 = b_2 = 1$ also at $Pr = 1$).

According to Owen and Rogers [4,5], the integral parameter $K_V$ is equal to 0.3482 in the laminar flow (for turbulent flow see Eq. (25)).

With allowance for the aforementioned relations for parameters in the right-hand side of Eq. (27), it is easy to see that

$$\chi = C_\chi x^{m_x - m - 1}, \quad C_\chi = \frac{K_1}{A_c(1+\alpha^2)^{1/2}Pr} \tag{29}$$

Apparently, solution (3) for the temperature distribution (1), (2) takes place at $m_x^* = m_x - m = 1$, $m_x = 1 + m$.

Eq. (28) can be expressed using Eqs. (29) in the following form

$$K_H = a_* + b_* x^{m_x^* - 1} \tag{30}$$

$$a_* = \frac{1}{b_2}, \qquad b_* = -Pr^{n_p}(1-K_V)\frac{b_1}{b_2}C_\chi \tag{31}$$

Dividing numerator and denominator of the integrand in the right-hand side of Eq. (27) by $x^{m_x^*}$, expressing $K_H$ from Eq. (30) one obtains for the integral in the right-hand side of Eq. (27)

$$\int_x^1 \frac{x^{m_x^*}\,\mathrm{d}x}{a_* x^2 + b_* x^{m_x^*+1}} = \frac{1}{b_*(1-m_x^*)}\ln\frac{a_* + b_* x^{m_x^*-1}}{a_* + b_*} = \ln\left[\frac{a_* + b_* x^{m_x^*-1}}{a_* + b_*}\right]^{\frac{1}{b_*(1-m_x^*)}} \tag{32}$$

One can also rewrite the left-hand side of Eq. (27) as follows

$$\left[\ln\left(Re_\omega\bar\delta K_H K_m\overline{\Delta T}\right)\right]_x^1 = \ln\left[\overline{\Delta T}\frac{K_H x^{2+m}}{K_{H_{x=1}}}\right]^{-1} \tag{33}$$

Substituting Eqs. (32) and (33) into Eq. (26), one can ultimately obtain

$$\overline{\Delta T} = \left[\frac{K_H}{K_{H_{x=1}}}\right]^{-\frac{K_1}{Pr\,K_m\gamma b_*(1-m_x^*)}-1} x^{-2-m} \tag{34}$$

## 4. Passage to the limiting case of $m_x^* = 1$

Let us consider limit of Eq. (34) at $m_x^* \to 1$ or, that is the same, at $y = 1 - m_x^* \to 0$ . Utilizing the rule of L'Hospital, one can obtain

$$\lim_{y\to 0} \frac{\ln \frac{a_* + b_* x^{-y}}{a_* + b_*}}{b_* y} = -\frac{\ln x}{a_* + b_*} = \ln x^{-\frac{1}{a_* + b_*}} \tag{35}$$

Arguments of logarithms in the right-hand sides of Eqs. (32) and (35) at $m_x^* \to 1$ become equal

$$\left[\frac{a_* + b_* x^{m_x^* - 1}}{a_* + b_*}\right]^{\frac{1}{b_*(1-m_x^*)}}_{m_x^*\to 1} = \left[\frac{K_H}{K_{H_{x=1}}}\right]^{\frac{1}{b_*(1-m_x^*)}}_{m_x^*\to 1} = x^{-\frac{1}{a_* + b_*}} \tag{36}$$

At $m_x^* \to 1$, solution (34) with allowance for relation (36) reduces to Eq. (1) with

$$n_* = \frac{K_1}{Pr\, K_m \gamma (a_* + b_*)} - 2 - m \tag{37}$$

If the value of $n_*$ is specified (as it has been done elsewhere), one can derive a formula for $K_1$, taking into account that $a_* + b_* = K_H$ at $m_x^* = 1$

$$K_1 = (2 + m + n_*)\gamma\, K_H K_m\, Pr \tag{38}$$

## 5. An extremum of the function $\overline{\Delta T}$

It is deemed important for the present examination to analyze some properties of solution (34). Having found the derivative of Eq. (34) with respect to coordinate $x$, it is possible to determine the coordinate of the point of an extremum for the temperature distribution (34)

$$x_{\text{ext}} = \left[\frac{\frac{K_1}{Pr\, K_m \gamma} - b_*(m_x + 1)}{a_*(2 + m)}\right]^{\frac{1}{1-m_x^*}} \tag{39}$$

Relative thickness of the thermal boundary layer $\Delta$ for the turbulent flow is found from the first of Eqs. (29) for $\chi$ and Eq. (22). Consequently, the value of $\Delta$ is

$$\Delta = \left(\chi\, Pr^{n_p}\right)^{-1/n} = \left(C_\chi x^{m_x^* - 1} Pr^{n_p}\right)^{-1/n} \tag{40}$$

For boundary conditions (1), (2), one can obtain $m_x^* = 1$ and $\Delta = \text{const}$. At $m_x^* < 1$, the value of $\Delta$ increases with $x$. At $m_x^* > 1$, the dependence of $\Delta$ on $x$ is decreasing.

Relation (30) for $K_H$ has a critical point $K_H = 0$. Basing on the physical sense of the model used, the parameter $K_H$ can be only positive. Thus, it follows for the critical point

$$\chi_{\text{crit}} = \frac{1}{b_1 Pr^{n_p}(1 - K_V)} \tag{41}$$

$$\Delta_{\text{crit}} = \left(\chi_{\text{crit}} Pr^{n_p}\right)^{-1/n} = \left[\frac{1}{b_1(1 - K_V)}\right]^{-1/n} \tag{42}$$

$$x_{\text{crit}} = [\chi_{\text{crit}}/C_\chi]^{\frac{1}{m_x^* - 1}} \tag{43}$$

Eqs. (40)–(43) are important in calculations of distributions of $\overline{\Delta T}$ and their analysis.

## 6. Computations of the Nusselt number and wall temperature distributions

Northrop [9] and Northrop and Owen [10] used the integral method of Dorfman [1] at the fixed value $n = 1/7$ for numerical simulations of the conditions observed in their own experiments. As well as in case of the analytical version of the Dorfman's method, the results of numerical predictions of the Nusselt number done by Northrop [9] and Northrop and Owen [10] noticeably exceeded their experimental data at $\mathrm{d}\overline{\Delta T}/\mathrm{d}x \approx 0$ and $\mathrm{d}\overline{\Delta T}/\mathrm{d}x < 0$. Agreement of the computations and experiments was good at $\mathrm{d}\overline{\Delta T}/\mathrm{d}x > 0$ except for the cases of high values of $Re_\varphi$, at which the predictions were lower than experimental values.

Ong and Owen [15] simulated the experimental conditions of Northrop [9] via a numerical solution of the boundary layer's differential equations with the use of the algebraic model of turbulent viscosity proposed by Cebeci and Smith [16]. Simulations and experiments agreed well. Therefore, this is the evidence that the experimental data of Northrop [9] are reliable, and the reason of difference in computations of Northrop [9] and Northrop and Owen [10] from the their own experiments consists indeed in the essential error of the Dorfman's method at $\mathrm{d}\overline{\Delta T}/\mathrm{d}x \leqslant 0$.

Selected for the analysis in this paper, as well as in the work of Ong and Owen [15], were the experimental data of Northrop [9] for the Nusselt number based on the local heat flux measurements with the use of fluxmeters. The resulting Nusselt numbers were further corrected by deduction of the radiant heat flux using the procedure of Northrop [9].

All our further computations were done at $Pr = 0.72$ as appropriate for air.

Experimental distributions of the temperature difference between the disk and the outer flow were classified by Northrop [9] into four groups. They are regarded as those conventionally featured by the formulas (1), (2) at $n_* = -0.2, 0.1, 0.4$ and $0.6$. Examples of such distributions are shown in Figs. 2, 4 and 6. Within each group, data for $\overline{\Delta T}$ differed from each other by maximum 10–15% for different values of $Re_\varphi$, with the general mode of the variation of $\overline{\Delta T}$ remaining practically the same.

Correspondence of Eq. (2) to the experiments at the above-mentioned values of the exponent $n_*$ is quite conventional. It is apparent, that Eq. (2) assumes absence of the points of a minimum or maximum (i.e., points of an extremum) and inflection inside a range of the definition of $T_w$ over the disk's radius. At the same time all experimental distributions plotted in Figs. 2, 4 and 6 exhibit the above-mentioned particular points. However, as a matter of a convenience of the references, the classification of the experiments into the groups accepted by Northrop [9] is preserved also in this paper.

Results of modeling the case conventionally named $n_* = 0.1$ are presented in Figs. 2, 3. Computations were done at $n = n_T = 1/6$. Distributions of the temperature head $\overline{\Delta T}$ correlate well with Eq. (2) at $n_* = 0.06$, $c_0^* = 1.16$

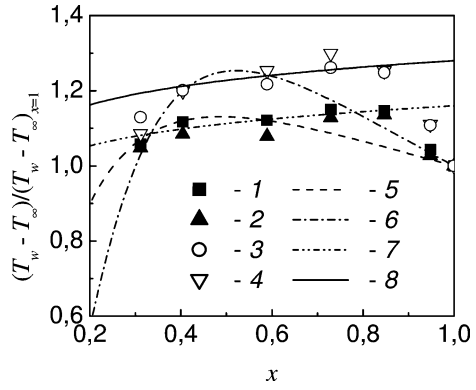


Fig. 2. Radial distribution of the temperature distribution $\overline{\Delta T}$, case conventionally $n_* = 0.1$. Experiments of Northrop [9]: 1—$Re_\varphi = 1.08 \times 10^6$; 2—$1.35 \times 10^6$; 3—$2.14 \times 10^6$; 4—$3.2 \times 10^6$. Calculations using Eq. (34) at $n = 1/6$: 5—$K_1 = 0.0232$, $m_x = 1.48$; 6—$K_1 = 0.0224$, $m_x = 1.38$. Eq. (2): 7—$c_0^* = 1.16$, $n_* = 0.06$; 8—$c_0^* = 1.26$, $n_* = 0.06$.

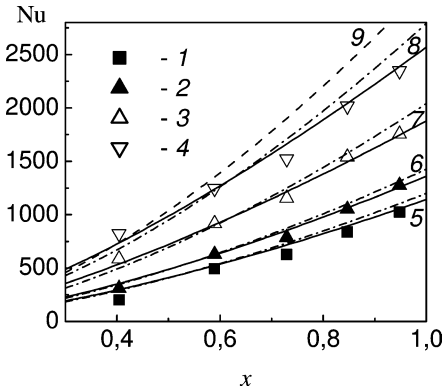


Fig. 3. Radial distribution of the Nusselt number, case conventionally $n_* = 0.1$: 1–4—experiments of Northrop [9]: 5–8—present predictions at $n = n_T = 1/6$. Solid lines, Eq. (9): 5, 6—$K_1 = 0.0232$, $m_x = 1.48$; 7, 8—$K_1 = 0.0224$, $m_x = 1.38$. Dash-dotted lines 5–8—Eqs. (3), (7), $K_1 = 0.0243$, $n_* = 0.06$. Dashed line 9—Eqs. (3), (5), $K_1 = 0.0197$, $n_* = 0.1$. Reynolds numbers: 1, 5—$Re_\varphi = 1.08 \times 10^6$; 2, 6—$1.35 \times 10^6$; 3, 7—$2.14 \times 10^6$; 4, 8, 9—$3.2 \times 10^6$.

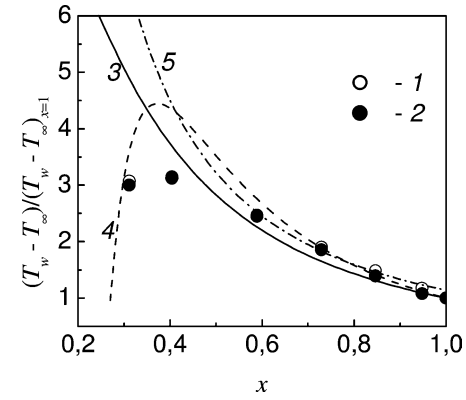


Fig. 4. Radial distribution of the temperature distribution $\overline{\Delta T}$, case conventionally $n_* = -0.2$. Experiments of Northrop [9]: 1—$Re_\varphi = 1.08 \times 10^6$; 2—$2.65 \times 10^6$. Calculations using Eq. (34) at $n = 1/6$: 3—$K_1 = 0.0157$, $m_x = 1.3$; 4—$K_1 = 0.0137$, $m_x = 0.775$. Calculations using Eq. (2): 5—$c_0^* = 1.14$, $n_* = -1.5$.

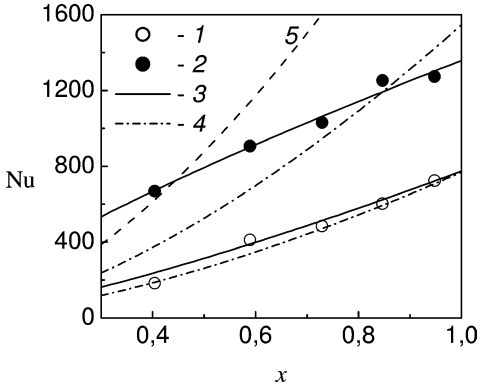


Fig. 5. Radial distribution of the Nusselt number, case conventionally $n_* = -0.2$: 1, 2—experiments of Northrop [9]: 3, 4—present predictions at $n = n_T = 1/6$. Lower group of lines 3, 4 and 1—$Re_\varphi = 1.08 \times 10^6$; upper group of lines 3, 4 and 5—$Re_\varphi = 2.65 \times 10^6$. Lower line 3—Eq. (9), $K_1 = 0.0157$, $m_x = 1.3$; upper line 3—Eq. (9), $K_1 = 0.0137$, $m_x = 0.775$. Lines 4—Eqs. (3), (7), $K_1 = 0.0156$, $n_* = -1.5$. Line 5—Eqs. (3), (5), $K_1 = 0.0193$, $n_* = -0.2$.

for $Re_\varphi = (1.08, \ldots, 1.35) \times 10^6$ and at $n_* = 0.06$, $c_0^* = 1.26$ for $Re_\varphi = (2.14, \ldots, 3.2) \times 10^6$ over the range $x \approx 0.3, \ldots, 0.85$. Resulting from this fact is fair consistency of the experimental values for the Nusselt number and those calculated from Eq. (3) (with $K_1$ being computed from Eq. (7)) for $x \approx 0.3, \ldots, 0.85$. However, observed for $x > (0.7, \ldots, 0.85)$ is the decreasing radial dependence of experimental values of the wall temperature contrary to the still increasing predicted values of $\overline{\Delta T}$ . This phenomenon generates the tendency of exceeding by the predicted Nusselt numbers over the experimental values in the area where signs of the derivatives $\mathrm{d}\overline{\Delta T}/\mathrm{d}x$ are in a disagreement. This tendency is amplified with the increasing Reynolds numbers $Re_\varphi$. It is also necessary to note that the calculation of Nu from Eq. (3) with the use of Eq. (7) for $K_1$ is still better than use of Eqs. (3) and (5) (Dorfman's [1] method) at $n_* = 0.1$, $n = n_T = 1/7$ (see curve 9 in Fig. 3).

Improvement of the correlation with the experimental data for the Nusselt number can be attained using Eq. (9) and simulating distributions of $\overline{\Delta T}$ using Eq. (34). As a whole, the absolute errors of Eq. (34) with respect to the experimental data are not lower than errors of Eq. (2). However, formula (2) predicts constant sign of the derivative $\mathrm{d}\overline{\Delta T}/\mathrm{d}x$ for any $x$. On the contrary, Eq. (34) allows the quite good simulation also of the sign of the derivative $\mathrm{d}\overline{\Delta T}/\mathrm{d}x$, which in the considered case changes from the positive to negative values with increasing $x$. This is the main reason of the improvement of the consistency between the predicted and experimental values of *Nu*.

Results of simulations of the case conventionally $n_* = -0.2$ are shown in Figs. 4, 5. Predictions using Eqs. (3), (7), (9) and (34) were done at $n = n_T = 1/6$. As evident from Fig. 4, a fair agreement of the predicted and experimental data for $\overline{\Delta T}$ is observed at $x \geqslant 0.6$. Only curve 4 exhibits qualitative consistency of the sign of the predicted deriva-

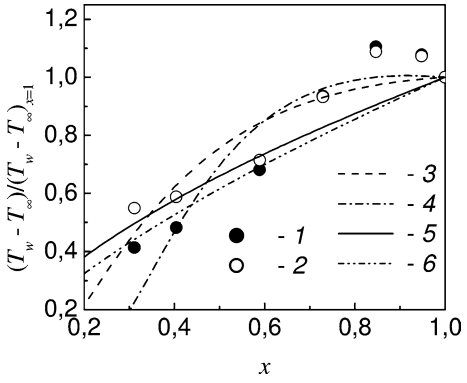


Fig. 6. Radial distribution of the temperature distribution $\overline{\Delta T}$, case conventionally $n_* = 0.4$ (data 1, 4, 6 at $Re_\varphi = 2.67 \times 10^6$) and $n_* = 0.6$ (data 2, 3, 5 at $Re_\varphi = 1.59 \times 10^6$). 1, 2—experiments of Northrop [9]. Computations, Eq. (34): 3—$K_1 = 0.0219$, $m_x = 1.48$, $n = 1/6.5$; 4—$K_1 = 0.0249$, $m_x = 1.34$, $n = 1/6$. Eq. (2): 5—$c_0^* = 1$, $n_* = 0.6$, 6—$c_0^* = 1$, $n_* = 0.7$.

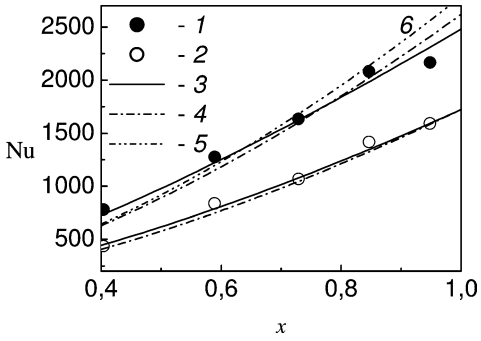


Fig. 7. Radial distribution of the Nusselt number, case conventionally $n_* = 0.4$ (upper group of lines, $Re_\varphi = 2.67 \times 10^6$) and $n_* = 0.6$ (lower group of lines, $Re_\varphi = 1.59 \times 10^6$). 1, 2—experiments of Northrop [9]; 3, 4—present predictions at $n = n_T = 1/6$ (upper group) and $n = n_T = 1/6.5$ (lower group). Lower line 3—Eq. (9), $K_1 = 0.0219$, $m_x = 1.48$; upper line 3—Eq. (9), $K_1 = 0.0249$, $m_x = 1.34$. Lower line 4—Eqs. (3), (7), $K_1 = 0.0227$, $n_* = 0.6$; upper line 4—Eqs. (3), (7), $K_1 = 0.0262$, $n_* = 0.7$. Line 5—Eqs. (3), (5), $K_1 = 0.0202$, $n_* = 0.4$.

tive $\mathrm{d}\overline{\Delta T}/\mathrm{d}x$ with the experiments at $x = 0.35, \ldots, 0.45$. It should be mentioned that the correlation of Eq. (2) with the experiments is observed only at $n_* = -1.5$, but not at $n_* = -0.2$, as suggested in the work of Northrop [9].

On the face of it, differences in distributions of $\overline{\Delta T}$ in Fig. 4 at $x \geqslant 0.6$ obtained from Eqs. (2) and (34) seem to be not too essential. However, it is evident that the Nusselt numbers are sensitive to the choice of the parameters $K_1$ and $m_x$. Values of *Nu* from Eqs. (3), (7) at $Re_\varphi = 1.08 \times 10^6$ show quite a good agreement with the experiments (the lower curve 4 in Fig. 5). However, the experimental point for *Nu* at $x \approx 0.4$ corresponds to the laminar flow, and an agreement with it means that the predicted dependence 4 should be considered underestimated. Confirming this fact is the upper curve 4 for $Re_\varphi = 2.65 \times 10^6$, where inadequate model (3), (7) results in an essential underestimation of the calculations at $x \leqslant 0.7$ as compared with experiments, with this underestimation being not "compensated" with an insufficient development of the turbulent flow in the experiments (i.e., the turbulent flow is already developed at $x \approx 0.4$).

Again, an improvement of the agreement with the experimental data for the Nusselt number is achieved due to Eq. (9), with the distributions $\overline{\Delta T}$ being modeled using Eq. (34). Parameters $K_1$ and $m_x$ in Eq. (34) were chosen based on the necessity of an agreement of the predicted and experimental values of *Nu*.

A calculation of the Nusselt number from Eq. (3) using the Dorfman's method (Eq. (5)) at $n_* = -0.2$ leads to obtaining the noticeably overestimated values of *Nu* in comparison with the experiments (curve 5 in Fig. 5).

Shown in Figs. 6, 7 are the results of the quite close cases conventionally $n_* = 0.4$ and $n_* = 0.6$. For $Re_\varphi = 1.59 \times 10^6$, a good agreement with the experiments is attained at $n = n_T = 1/6.5$; for $Re_\varphi = 2.67 \times 10^6$, it is necessary to employ values $n = n_T = 1/6$ (see lines 3 in Fig. 7). An analysis of the distributions of the temperature head $\overline{\Delta T}$ in Fig. 6 at $x = 0.3, \ldots, 0.6$ shows that indeed the value $n_* = 0.6$ at $c_0^* = 1$ in Eq. (2) correlates well with the experiments at $Re_\varphi = 1.59 \times 10^6$. At the same time, the experiments at $Re_\varphi = 2.67 \times 10^6$ can bee simulated better with the value $n_* = 0.7$, but not $n_* = 0.4$.

Eq. (34) allows obtaining distributions of $\overline{\Delta T}$ with an error not exceeding the error of Eq. (2) (see Fig. 6). However, Eq. (34) provides an essential radial variation of the absolute value of the derivative $\mathrm{d}\overline{\Delta T}/\mathrm{d}x$ and thus more opportunities for a selection of the parameters $K_1$ and $m_x$.

An analysis of the distributions of the local Nusselt numbers in Fig. 7 shows that Eqs. (9) together with (34) at specially fitted values $K_1$ and $m_x$ provide a better agreement with the experiment than Eqs. (3) together with (7) do. This is especially obvious for the higher values $Re_\varphi = 2.67 \times 10^6$. Inexactitudes of Eq. (3) at $K_1$ computed from Eq. (5) are not so essential (see curve 6 in Fig. 7). This fact corresponds to the earlier obtained conclusions of Shevchuk [12,13] that the errors of the Dorfman's (1963) method are essential at $n_* \leqslant 0$.

It is also necessary to mention that the predictions in Figs. 3, 5 and 7 correlate well with calculations of Ong and Owen [15] done, as indicated above, using a differential method.

The characteristic feature of data in Figs. 3, 5 and 7 is the "dip" of the experimental values of *Nu* in the work of Northrop [9] at the point $x \approx 0.73$ as compared to predictions. The same inconsistency of the experiments and predictions at the position $x \approx 0.73$ is pointed out by Ong and Owen [15]; apparently, the reason is the systematic error of the experimental measurements of Northrop [9] in this location.

It is necessary to emphasize that the velocity and temperature profiles were not measured in the experiments of Northrop [9], therefore the fulfilled estimation of the values of the exponents $n$ is grounded on the oblique data for the Nusselt numbers. Nevertheless, taking into account the interrelation of the values $n$ and the exponent $n_R$ at the Reynolds number in Eq. (3) for *Nu* under condition (1) or

(2) (see Table 1), it is possible to deem the analysis given justified. Apparently, the rate of the radial increase of the Nusselt numbers $Nu$ in Figs. 3, 5 and 7 corresponds to the smaller values of $n_R$ and $m$ and, consequently, to the higher values of $n$, that is confirmed by the computations presented here. Besides, it is interesting to point out that Elkins and Eaton (1997), who measured experimentally the temperature distributions in the boundary layer at the negative value of $\mathrm{d}\overline{\Delta T}/\mathrm{d}x$ in the case $q_w = \text{const}$ (or $n_* \approx -0.6$), obtained values $n = 1/4, \ldots, 1/5$ for the temperature profiles at $Re_\omega = 10^6$. This is consistent with the results of the presents research at $n_* = -0.2$.

## 7. Conclusions

A new analytical solution of the problem under consideration given by Eqs. (9) for the Nusselt number and (34) for $\overline{\Delta T}$ provides much better accuracy of the agreement with the experiments in the majority of the cases considered, than the previously known solution (2) and (3) do. The solution of the inverse problem presented by Eqs. (9), (34) comprises much wider range of possible boundary conditions for the surface temperature distribution $\overline{\Delta T}$ than the solution of the direct problem (2), (3). It should be expected that the solutions analogous to Eqs. (9), (34) can be found for a variety of the other problems of fluid flow and heat transfer.

## Acknowledgements

The research results that laid the foundation of the present work were obtained in part due to support of the Research Fellowship of the Alexander von Humboldt Foundation, which is gratefully acknowledged.

## References

[1] L.A. Dorfman, Hydrodynamic Resistance and the Heat Loss of Rotating Solids, Oliver and Boyd, Edinburgh, 1963.
[2] G. Cardone, T. Astarita, G.M. Carlomagno, Infrared heat transfer measurements on a rotating disk, Optical Diagnostics Eng. 1 (2) (1996) 1–7.
[3] C.J. Elkins, J.K. Eaton, Heat transfer in the rotating disk boundary layer, Stanford University, Department of Mechanical Engineering, Thermosciences Division Report TSD-103, 1997.
[4] J.M. Owen, R.H. Rogers, Flow and Heat Transfer in Rotating-Disc Systems, vol. 1: Rotor-Stator Systems, Research Studies Press/Wiley, Taunton/New York, 1989.
[5] J.M. Owen, R.H. Rogers, Flow and Heat Transfer in Rotating-Disc Systems, vol. 2: Rotating Cavities, Research Studies Press/Wiley, Taunton/New York, 1995.
[6] E.C. Cobb, O.A. Saunders, Heat transfer from a rotating disk, Proc. Roy. Soc. A 236 (1956) 343–351.
[7] N.I. Nikitenko, Experimental investigation of heat exchange of a disc and a screen, J. Engrg. Phys. 6 (6) (1963) 1–11.
[8] S.T. McComas, J.P. Hartnett, Temperature profiles and heat transfer associated with a single disc rotating in still air, in: U. Grigull, E. Hahne (Eds.), Proceedings of the 4th Internat. Heat Transfer Conference, Paris-Versailles, France, Elsevier, Amsterdam, 1970, Paper FC 7.7.
[9] A. Northrop, Heat transfer in a cylindrical rotating cavity, Ph.D. Thesis, University of Sussex, Brighton, UK, 1984.
[10] A. Northrop, J.M. Owen, Heat transfer measurements in rotating-disc systems. Part 1: The free disc, Internat. J. Heat Fluid Flow 9 (1988) 19–26.
[11] Cz.O. Popiel, L. Boguslawski, Local heat-transfer coefficients on the rotating disk in still air, Internat. J. Heat Mass Transfer 18 (1975) 167–170.
[12] I.V. Shevchuk, Effect of the wall temperature on laminar heat transfer in a rotating disk: An approximate analytical solution, High Temperature 39 (2001) 637–639.
[13] I.V. Shevchuk, Turbulent heat transfer of rotating disk at constant temperature or density of heat flux to the wall, High Temperature 38 (2000) 499–501.
[14] I.V. Shevchuk, N. Saniei, X.T. Yan, Impingement heat transfer over a rotating disk: Integral method, AIAA J. Thermophys. Heat Transfer 17 (2003) 291–293.
[15] C.L. Ong, J.M. Owen, Computation of the flow and heat transfer due to a rotating disc, Internat. J. Heat Fluid Flow 12 (1991) 106–115.
[16] T. Cebeci, A.M.O. Smith, Analysis of Turbulent Boundary Layers, Academic Press, New York, 1974.